



Article

In Vitro Antitumor Active Gold(I) Triphenylphosphane Complexes Containing 7-Azaindoles

Pavel Štarha¹, Zdeněk Trávníček^{1,*}, Bohuslav Drahoš¹ and Zdeněk Dvořák²

¹ Department of Inorganic Chemistry, Regional Centre of Advanced Technologies and Materials, Faculty of Science, Palacký University Olomouc, 17. listopadu 12, 771 46 Olomouc, Czech Republic; pavel.starha@upol.cz (P.S.); bohuslav.drahos@upol.cz (B.D.)

² Department of Cell Biology and Genetics, Regional Centre of Advanced Technologies and Materials, Faculty of Science, Palacký University Olomouc, Šlechtitelů 27, 783 71 Olomouc, Czech Republic; zdenek.dvorak@upol.cz

* Correspondence: zdenek.travnicek@upol.cz; Tel.: +420-585-634-352

Academic Editor: Nick Hadjiladis

Received: 3 October 2016; Accepted: 30 November 2016; Published: 11 December 2016

Abstract: A series of gold(I) complexes of the general composition $[\text{Au}(naza)(\text{PPh}_3)]$ (1–8) was prepared and thoroughly characterized (e.g., electrospray ionization (ESI) mass spectrometry and multinuclear nuclear magnetic resonance (NMR) spectroscopy). The N1-deprotonated anions of 7-azaindole or its derivatives (*naza*) are coordinated to the metal centre through the N1 atom of their pyrrole ring, as proved by a single crystal X-ray analysis of the complexes $[\text{Au}(3I5Braza)(\text{PPh}_3)]$ (7) and $[\text{Au}(2Me4Claza)(\text{PPh}_3)] \cdot \frac{1}{2}\text{H}_2\text{O}$ (8'). The in vitro cytotoxicity of the complexes 1–8 was studied against both the *cisplatin*-sensitive and -resistant variants of the A2780 human ovarian carcinoma cell line, as well as against the MRC-5 human normal fibroblast cell line. The complexes 4, 5, and 8, containing deprotonated 3-iodo-7-azaindole, 5-bromo-7-azaindole, and 2-methyl-4-chloro-7-azaindole (2Me4Claza), respectively, showed significantly higher potency ($\text{IC}_{50} = 2.8\text{--}3.5 \mu\text{M}$) than *cisplatin* ($\text{IC}_{50} = 20.3 \mu\text{M}$) against the A2780 cells and markedly lower effect towards the MRC-5 non-cancerous cells ($\text{IC}_{50} = 26.0\text{--}29.2 \mu\text{M}$), as compared with the mentioned A2780 cancer cells. The results of the flow cytometric studies of the A2780 cell cycle perturbations revealed a G₂-cell cycle phase arrest of the cells treated by the representative complexes 1 and 5, which is indicative of a different mechanism of action from *cisplatin* (induced S-cell cycle phase arrest). The stability of the representative complex 8 in the water-containing solution as well as its ability to interact with the reduced glutathione, cysteine and bovine serum albumin was also studied using ¹H and ³¹P-NMR spectroscopy (studied in the 50% DMF-*d*₇/50% D₂O mixture) and ESI+ mass spectrometry (studied in the 50% DMF/50% H₂O mixture); DMF = dimethylformamide. The obtained results are indicative for the release of the N-donor azaindole-based ligand in the presence of the used biomolecules.

Keywords: gold(I) complexes; 7-azaindole; triphenylphosphane; crystal structures; antitumor activity; in vitro

1. Introduction

Transition metal complexes offer a wide pallet of biological activities, including the anticancer or anti-inflammatory ones [1–3]. Several complexes, as it is known especially for platinum-based anticancer drugs [4], are in use in medical practice. Among the non-platinum complexes, several gold(I) complexes, such as triethylphosphane-(2,3,4,6-tetra-*O*-acetyl-β-D-thiopyranosato)gold(I) complex (*auranofin*; $[\text{Au}(\text{SATg})(\text{PEt}_3)]$), are clinically used for the treatment of rheumatoid arthritis [5]. However, many gold(I) complexes (including *auranofin*) have recently been reported and frequently patented

as antitumor active substances [5–8]. The published results revealed that various gold(I) complexes: (a) exceed activity of platinum-based drugs; (b) effectively overcome the tumour cell resistance to *cisplatin*; and (c) act through different mechanisms of action from the conventional platinum-based drugs. The above-mentioned *auranofin* successfully completed the Phase I and II of the clinical trials as the anticancer drug for the treatment of chronic lymphocytic leukaemia (CLL) [9,10], other clinical studies using *auranofin* for the treatment of different types of cancer (e.g., ovarian carcinoma) are in progress [11].

The mechanism of action of anticancer gold(I) complexes, although still not fully understood, seems to involve the inhibition of the glutathione reductase-like enzyme thioredoxin reductase (TrxR) [12]. However, it is well-known for *auranofin* and other substituted-phosphane-gold(I) complexes, such as $[\text{AuCl}(\text{PPh}_3)]$, that these agents release their *S*-donor ligands (*auranofin* $[\text{Au}(\text{SATg})(\text{PEt}_3)]$) or chlorido ($[\text{AuCl}(\text{PPh}_3)]$) ligand under the physiological conditions to form $[\text{Au}(\text{PR}_3)]^+$ species which react easily with various biomolecules, such as albumin (AlbH) or glutathione (GSH) [5,13,14]. For example, the interaction of $[\text{AuCl}(\text{PPh}_3)]$ with the mixture of GSH and 5,5'-dithiobis-2-nitrobenzoic acid (dtnb) provided the $[\text{Au}(\text{PPh}_3)(\text{SG})]$ adduct [15]. Interestingly, even the phosphane-based ligand (PR_3) can be released when the original gold(I) complex interacts with the mentioned biomolecules, as proved for *auranofin* and $[\text{AuCl}(\text{PPh}_3)]$, to form species, such as $[\text{Au}(\text{SG})_2]^-$ or $[\text{Au}(\text{Alb})_2]^-$. On the other hand, several highly potent anticancer gold(I) complexes, e.g., $[\text{AuCl}(\text{NHC})]$ or $[\text{Au}(\text{NHC})(\text{PPh}_3)]$ were found to be inert to GSH [16–18], indicating that the above-mentioned ligand replacement is not most likely the necessary activation step of biologically active gold(I) complexes (NHC stands for C-donor 1,3-diethylbenzimidazol-2-ylidene carbene ligand).

Recently, our research group reported the triphenylphosphane-gold(I) complexes containing *N*6-benzyladenine-, hypoxanthine- and 9-deazahypoxanthine-derived *N*-donor ligands (HL), $[\text{Au}(\text{L})(\text{PPh}_3)]$, which exhibited high cytotoxicity, ability to overcome acquired resistance to *cisplatin*, selectivity towards cancer cells over the normal ones and/or high anti-inflammatory activity [19–22]. In this work, we report on new complexes of the general composition $[\text{Au}(n\text{aza})(\text{PPh}_3)]$ (1–8) containing the *N*1-deprotonated, *C*2-, *C*3-, *C*4-, and/or *C*5-substituted 7-azaindole-based ligands (*naza*; Figure 1). 7-Azaindole itself (i.e., unsubstituted; Haza), as well as its halogeno-derivatives used in this work, are known as suitable ligands for various transition metal complexes [23,24], where they mostly act as electroneutral *N*7-coordinated ligand (e.g., $[\text{Pt}(\text{ox})(\text{Haza})_2]$, *cis*- $[\text{Pt}(3\text{ClHaza})_2\text{Cl}_2]$ or $[(\eta^6\text{-}p\text{-cym})\text{Ru}(\text{Haza})\text{Cl}_2]$; ox = oxalate(2–), *p*-cym = *p*-cymene) [25–27] or *N*1-monodentate (e.g., $[\text{Au}(\text{aza})(\text{PPh}_3)]$; 1 in this work), or *N*1,*N*7-bidentate-coordinated (e.g., $[\text{Cu}_2(\mu\text{-aza})_4(\text{dmf})_2]$) *N*1-deprotonated 7-azaindolate anions [28,29].

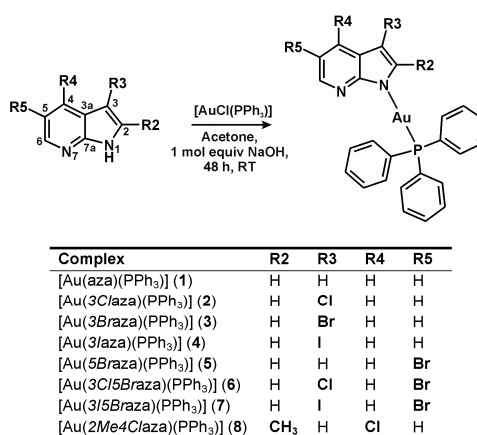


Figure 1. Synthetic pathway for the preparation of $[\text{Au}(n\text{aza})(\text{PPh}_3)]$ (1–8), the structural formulas of the used 7-azaindoles (*n*Haza) and the studied complexes 1–8, with atom numbering scheme and with a table summarizing the substituents of the 7-azaindole moiety for the used *n*Haza derivatives.

2. Results

2.1. Chemistry

In this work, we report on a series of eight triphenylphosphane-gold(I) complexes of the general formula $[\text{Au}(n\text{aza})(\text{PPh}_3)]$ (**1–8**), which were synthesized, thoroughly characterized in the solid state as well as in solution, and their in vitro cytotoxicity against both cancer and normal (i.e., non-cancerous) cell lines was studied, together with basic mechanistic aspects of their cytotoxic action. The complexes **1–8** were prepared in acetone from $[\text{AuCl}(\text{PPh}_3)]$ using a general procedure, as previously described in the literature for similar triphenylphosphane-gold(I) complexes containing heterocyclic *N*-donor ligands different from 7-azaindole (Figure 1) [19–22,30]. The used 7-azaindoles (*Hnaza*) were deprotonated in situ by an equimolar amount of NaOH. The products were isolated in good yields ($\approx 70\%$) and acceptable purity ($>95\%$), as proved by $^1\text{H-NMR}$ and $^{31}\text{P-NMR}$ spectroscopy; NMR = nuclear magnetic resonance. The studied substances are well-soluble in acetone, dimethylformamide (DMF), dimethyl sulfoxide (DMSO), chloroform, methanol, and ethanol, but the solubility in water was found to be very low. Complexes were stable in $\text{DMF-}d_7$ used for the NMR studies, because no changes were observed in the $^1\text{H-NMR}$ and $^{31}\text{P-NMR}$ spectra of **1–8** even after one week of standing at ambient temperature.

The N1–H hydrogen atoms of the used 7-azaindoles (*nHaza*), detected at ca. 12 ppm in their $^1\text{H-NMR}$ spectra, were not found in the $^1\text{H-NMR}$ spectra of the corresponding $[\text{Au}(n\text{aza})(\text{PPh}_3)]$ complexes, as a consequence of deprotonation of these organic molecules by 1 M NaOH (Figures S1 and S2). The aromatic hydrogens of **1–8**, as well as the hydrogen atoms of the methyl group of the complex **8**, were found in the $^1\text{H-NMR}$ spectra. The PPh_3 hydrogen atoms were detected at ca. 7.7 ppm. All of the $^1\text{H-NMR}$ aromatic C–H signals of the used 7-azaindoles shifted to higher fields after their coordination to the Au(I) atom, resulting in the negative coordination shift values ($\Delta\delta = \delta_{\text{complex}} - \delta_{\text{ligand}}$; ppm). Regarding the $^{13}\text{C-NMR}$ coordination shifts, high values ($\Delta\delta = 6.7\text{--}11.7$ ppm), calculated for the C2 and C7a carbons adjacent to the N1 nitrogen atom (Figure 1), are consistent with the N1-coordination mode of the used *naza* ligands. The N1-coordination mode was further proved by higher $^{15}\text{N-NMR}$ coordination shift of N1 (48.0 ppm) than N7 (-0.8 ppm), as observed for the representative complex **5**. The $^{31}\text{P-NMR}$ spectra of the studied complexes contained only one signal at ca. 33 ppm, assignable to the *P*-coordinated PPh_3 molecule.

The positive mode electrospray ionization (ESI+) mass spectra of the complexes **1–8** contained, except for the most intensive peaks of the $[\text{Au}(\text{PPh}_3)_2]^+$ species (100% relative intensity) at ca. 721.2 *m/z*, the characteristic molecular peaks of $\{[\text{Au}(n\text{aza})(\text{PPh}_3)] + \text{H}\}^+$ (2%–10% relative intensity) and the peaks of $[\text{Au}(\text{PPh}_3)]^+$ and free $\{(\text{Hnaza}) + \text{H}\}^+$ (see Supplementary Materials and Figure S3). The peaks of the $[\text{Au}(n\text{aza})_2]^-$ and $(n\text{aza})^-$ species were detected in the ESI– mass spectra of **1–8**.

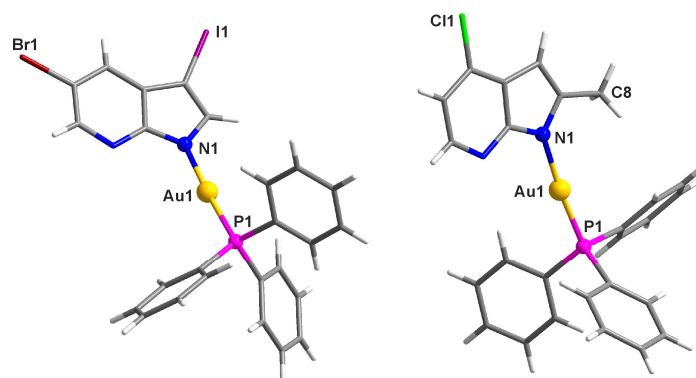
Both the Fourier transform infrared (FTIR) and Raman spectra of the complexes **1–8** contained, similarly to the spectra of uncoordinated *Hnaza*, the intensive peaks at $1574\text{--}1590\text{ cm}^{-1}$ and $1463\text{--}1481\text{ cm}^{-1}$, assignable to the $\nu(\text{C-N})_{\text{ring}}$ and $\nu(\text{C-C})_{\text{ring}}$ stretching vibrations, respectively [25,26]. Other peaks detected in the spectra at ca. $2900\text{--}3100\text{ cm}^{-1}$ belong to the $\nu(\text{C-H})_{\text{ar}}$ of the *naza* and PPh_3 ligands [19,25,26,31,32]. The maxima of the peaks belonging to the $\nu(\text{Au-N})$ and $\nu(\text{Au-P})$ vibrations were centred at ca. $479\text{--}501\text{ cm}^{-1}$ and $319\text{--}330\text{ cm}^{-1}$, respectively [19,31,32].

2.2. Single Crystal X-ray Analysis

Two representative complexes, $[\text{Au}(3\text{I}5\text{Braza})(\text{PPh}_3)]$ (**7**) and $[\text{Au}(2\text{Me}4\text{Claza})(\text{PPh}_3)] \cdot \frac{1}{2}\text{H}_2\text{O}$ (**8'**), were characterized by single crystal X-ray analysis. Crystal data and structure refinement parameters are given in Table 1. The molecular structures of **7** and **8'** are depicted in Figure 2, while the selected bond lengths and angles can be found in Table 2.

Table 1. Crystal data and structure refinements for the complexes [Au(3I5Braza)(PPh₃)] (**7**) and [Au(2Me4Claza)(PPh₃)]·½H₂O (**8'**).

	7	8'
Empirical Formula	C₂₅H₁₈AuBrIN₂P	C₅₂H₄₄Au₂Cl₂N₄OP₂
Formula weight	781.16	1267.68
Temperature (K)	120(2)	120(2)
Wavelength (Å)	0.71073	0.71073
Crystal system, space group	Monoclinic, <i>P</i> 2 ₁ / <i>c</i>	Monoclinic, <i>C</i> 2/ <i>c</i>
Unit cell dimensions		
<i>a</i> (Å)	6.8563(3)	24.2844(14)
<i>b</i> (Å)	24.2482(12)	15.1186(14)
<i>c</i> (Å)	14.7081(8)	16.3330(14)
α (°)	90	90
β (°)	101.313(2)	128.203(4)
γ (°)	90	90
<i>V</i> (Å ³)	2397.8(2)	4712.3(7)
<i>Z</i> , <i>D</i> _{calc} (g·cm ⁻³)	4, 2.164	4, 1.787
Absorption coefficient (mm ⁻¹)	9.172	6.444
Crystal size (mm)	0.170 × 0.140 × 0.120	0.160 × 0.120 × 0.120
<i>F</i> (000)	1456	2456
θ range for data collection (°)	2.825 to 27.513	2.500 to 27.940
Index ranges (<i>h</i> , <i>k</i> , <i>l</i>)		
	−7 ≤ <i>h</i> ≤ 8	−31 ≤ <i>h</i> ≤ 31
	−31 ≤ <i>k</i> ≤ 31	−19 ≤ <i>k</i> ≤ 19
	−19 ≤ <i>l</i> ≤ 19	−21 ≤ <i>l</i> ≤ 21
Reflections collected/unique	56041	104819
Data/restraints/parameters	5508/0/280	5648/0/289
Goodness-of-fit on <i>F</i> ²	1.071	1.012
Final <i>R</i> indices [<i>I</i> > 2σ(<i>I</i>)]	<i>R</i> ₁ = 0.0279, <i>wR</i> ₂ = 0.0453	<i>R</i> ₁ = 0.0193, <i>wR</i> ₂ = 0.0340
<i>R</i> indices (all data)	<i>R</i> ₁ = 0.0427, <i>wR</i> ₂ = 0.0485	<i>R</i> ₁ = 0.0301, <i>wR</i> ₂ = 0.0366
Largest peak and hole (e Å ⁻³)	0.900 and −1.237	0.550 and −0.702
Cambridge Crystallographic Data Centre nos.	1507789	1507790

**Figure 2.** The molecular structures of [Au(3I5Braza)(PPh₃)] (**7**; left) and [Au(2Me4Claza)(PPh₃)]·½H₂O (**8'**; right), the ½H₂O molecule of crystallization was omitted for clarity.

Both the complexes **7** and **8'** adopted the slightly distorted linear geometry. The Au1–N1 and Au1–P1 bond lengths, as well as the P1–Au1–N1 bond angle values (see Table 2) fall within the ranges of 1.97–2.12 Å (average of 2.06(3) Å) and 2.21–2.28 Å (average of 2.235(8) Å), and 168.4–179.6° (average of 175(2)°), respectively, in agreement with similar triphenylphosphane-gold(I) complexes containing heterocyclic *N*-donor ligands, e.g., [21,22,28], deposited in the Cambridge Crystallographic Data Centre (CCDC; version 5.37 updated to May 2016 [33]). For the previously reported X-ray structure of [Au(aza)(PPh₃)] (**1** in this work) [28], its P1–Au1–N1 bond angle value of 176.6° is consistent with the value of **7**, but differs markedly from that of **8'**. Regarding the bond lengths, Au1–N1 of **7** is

higher than those of **8'** (Table 2) and [Au(aza)(PPh₃)] (**1** in this work; 2.033(4) Å) [28], while the Au1–P1 bond lengths of **7**, **8'** (Table 2) and [Au(aza)(PPh₃)] (2.2321(12) Å) do not differ markedly.

Table 2. Selected bond lengths (Å) and angles (°) for the complexes [Au(3I5Braza)(PPh₃)] (**7**) and [Au(2Me4Claza)(PPh₃)]·½H₂O (**8'**).

Parameter	7	8'
Au1–N1	2.047(3)	2.030(2)
Au1–P1	2.2349(9)	2.2277(6)
P1–Au1–N1	176.41(8)	173.27(6)
Au1–P1–C10	112.34(12)	107.47(8)
Au1–P1–C20	111.24(12)	117.05(8)
Au1–P1–C30	115.36(11)	114.19(8)
Au1–N1–C2	126.1(2)	125.1(2)
Au1–N1–C7a	125.9(2)	127.7(2)

The crystal structure of **7** is stabilized by C–H···Br, C–H···I, C–H···C, C–H···N, C–H···π, and C···C non-covalent interactions (Table S1, Figure S4) [34,35]. In the case of **8'**, the O–H···N hydrogen bonds were detected between the N7 nitrogen atom of the 7-azaindole moiety and water molecule of crystallization, which together with C–H···O and C–H···C non-covalent contacts stabilize the crystal structure of this gold(I) complex (Table S1, Figure S5).

2.3. Aqueous Chemistry and Interaction Studies

2.3.1. Solution Behaviour in a Water/DMF Mixture

The representative complex **8** was found to be hydrolytically stable based on the ¹H and ³¹P-NMR results, when dissolved in the 50% DMF-*d*₇/50% D₂O mixture. Only one set of ¹H-NMR signals (e.g., C3–H signal at 6.50 ppm) and one ³¹P-NMR signal (34.8 ppm) were detected on the fresh solution, and no changes were observed even after 48 h of standing at ambient temperature. The positions of the ¹H and ³¹P-NMR signals detected on the solution of **8** in the 50% DMF-*d*₇/50% D₂O mixture were different from those of free H2Me4Claza (C3–H signal at 6.32 ppm; Figure 3), PPh₃ (³¹P-NMR signal at –4.7 ppm), the oxidized triphenylphosphane (O=PPh₃; ³¹P-NMR signal at 32.4 ppm) or [AuCl(PPh₃)] (³¹P-NMR signal at 34.2 ppm) dissolved in the same mixture of solvents (Figure S6).

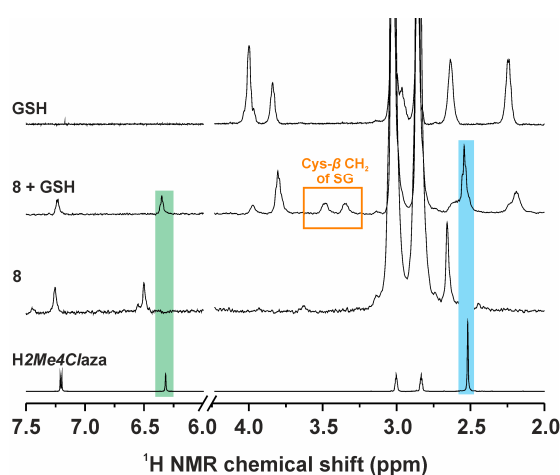


Figure 3. Proton nuclear magnetic resonance (¹H-NMR) spectra of [Au(2Me4Claza)(PPh₃)] (**8**) and its mixture with reduced glutathione (**8** + GSH) recorded after 48 h of standing at ambient temperature, given together (for comparative purposes) with the ¹H-NMR spectra of free H2Me4Claza and GSH. All samples were studied in the 50% DMF-*d*₇/50% D₂O solution. Green: C3–H signal of H2Me4Claza; blue: CH₃ signal of H2Me4Claza.

2.3.2. Interaction Studies with Biomolecules

The new $^1\text{H-NMR}$ signals of Cys- β CH_2 at 3.35 and 3.48 ppm, assignable to the S-deprotonated glutathione (i.e., SG) coordinated to the Au(I) atom through its sulphur atom, were detected immediately in the mixture of **8** and GSH (1 mol equiv), showing the formation of the $[\text{Au}(\text{PPh}_3)(\text{SG})]$ adduct (Figure 3). The position of the $^{31}\text{P-NMR}$ signal of **8** shifted from 34.8 ppm to 40.8 ppm, belonging most likely to the $[\text{Au}(\text{PPh}_3)(\text{SG})]$ adduct (Figure S6). The characteristic C3–H signal of the free ligand (i.e., H2Me4Claza) was found at 6.35 ppm in the $^1\text{H-NMR}$ spectra of the mixture of **8** and GSH (Figure 3). Neither new signals nor changes of intensity of the detected signals were observed after 48 h of standing at ambient temperature. Similar experiment performed with 5 mol equiv of GSH led to the same results (Figures S6 and S7). The peaks of the $\{[\text{Au}(\text{PPh}_3)(\text{SG})] + \text{H}\}^+$ adduct (overlapped with $\{[\text{Au}(\text{PPh}_3)(\text{SG})] + 2\text{H}\}^+$ in a 1.75:1.00 ratio) and the $\{[\text{Au}(\text{PPh}_3)(\text{SG})] + \text{Na}\}^+$ adduct (overlapped with $\{[\text{Au}(\text{PPh}_3)(\text{SG})] + \text{H} + \text{Na}\}^+$ in a 1.25:1.00 ratio) were found at 765.9 m/z (calcd. 766.1 m/z) and 789.1 m/z (calcd. 789.1 m/z), respectively, with the appropriate isotopic distribution pattern.

Regarding the interaction studies with cysteine (Cys), the $^1\text{H-NMR}$ signals of β CH_2 of the coordinated deprotonated cysteine (Cys^-) are clearly detectable at 3.44 and 3.63 ppm. The $^{31}\text{P-NMR}$ signal was detected at 40.6 ppm for the $[\text{Au}(\text{Cys}^-)(\text{PPh}_3)]$ adduct, that is at negligibly higher field than for the $[\text{Au}(\text{PPh}_3)(\text{SG})]$ adduct (see above). The C3–H $^1\text{H-NMR}$ signal of the released H2Me4Claza was found at 6.36 ppm (Figure S8). Any other changes were not observed after 48 h of standing at ambient temperature, as well as in the presence of an excess (5 mol equiv) of Cys interacting with **8**.

An interaction of **8** with bovine serum albumin (BSA) resulted immediately in a white turbidity, which was subsequently removed by centrifugation (13,000 rpm for 3 min; Mini Spin, Eppendorf AG, Hamburg, Germany). The $^1\text{H-NMR}$ spectrum recorded on the obtained supernatant contained the signals of the released N-donor ligand, with the signal positions (e.g., C3–H signal at 6.36 ppm) being consistent with those detected for free H2Me4Claza in the same mixture of solvents (Figure S8). No signals were detected in the $^{31}\text{P-NMR}$ spectra recorded on the mentioned supernatant. On the other hand, after the centrifuged turbidity was dissolved in DMF- d_7 , two $^{31}\text{P-NMR}$ signals were detected on this solution at 32.8 and 27.3 ppm, which suggested the formation two different species, including the BSA adduct with an Au–PPh₃ residue.

2.4. In Vitro Antitumor Activity

The complexes **1–8** were studied for their in vitro cytotoxicity against two human cancer cell lines (A2780 and A2780R) and one human non-cancerous cell line (MRC-5) (Table 3).

Table 3. The results of the in vitro cytotoxicity studies of gold(I) complexes **1–8** (and *cisplatin* for comparative purposes) against the human A2780 ovarian carcinoma, A2780R *cisplatin*-resistant ovarian carcinoma and MRC-5 normal fibroblast cell lines, performed with the 24 h exposure time. Data are expressed as half maximal inhibitory concentration (IC_{50}) \pm standard deviation (SD) (μM). The significant differences between the IC_{50} values for **1–8** and *cisplatin* are given as *** $p < 0.005$.

Complex	A2780	A2780R	MRC5	RF ¹	SI ²
$[\text{Au}(\text{aza})(\text{PPh}_3)]$ (1)	3.8 \pm 1.1 ***	4.4 \pm 0.8	7.7 \pm 1.7	1.2	2.0
$[\text{Au}(3\text{Claza})(\text{PPh}_3)]$ (2)	22.4 \pm 5.7	21.7 \pm 0.8	31.4 \pm 4.9	1.0	1.4
$[\text{Au}(3\text{Braza})(\text{PPh}_3)]$ (3)	23.3 \pm 3.4	21.3 \pm 0.8	27.3 \pm 1.7	0.9	1.2
$[\text{Au}(3\text{laza})(\text{PPh}_3)]$ (4)	3.5 \pm 0.4 ***	11.0 \pm 4.7	29.2 \pm 5.9	3.1	8.3
$[\text{Au}(5\text{Braza})(\text{PPh}_3)]$ (5)	3.1 \pm 0.5 ***	14.4 \pm 3.3	26.0 \pm 4.2	4.6	8.4
$[\text{Au}(3\text{Cl5Braza})(\text{PPh}_3)]$ (6)	22.9 \pm 2.3	13.8 \pm 2.1	26.5 \pm 3.7	0.6	1.2
$[\text{Au}(3\text{l5Braza})(\text{PPh}_3)]$ (7)	20.2 \pm 2.5	22.1 \pm 0.3	27.3 \pm 2.6	1.1	1.4
$[\text{Au}(2\text{Me4Claza})(\text{PPh}_3)]$ (8)	2.8 \pm 0.7 ***	8.9 \pm 3.8	26.9 \pm 3.6	3.2	9.6
<i>Cisplatin</i>	20.3 \pm 2.3	>50.0	>50.0	-	-

¹ RF = resistance factor (calculated as $\text{IC}_{50}(\text{A2780R})/\text{IC}_{50}(\text{A2780})$); ² SI = selectivity index (calculated as $\text{IC}_{50}(\text{MRC5})/\text{IC}_{50}(\text{A2780})$).

The complexes **1**, **4**, **5**, and **8** were significantly more effective ($p < 0.005$) against the A2780 cells ($\text{IC}_{50} = 2.8\text{--}3.8 \mu\text{M}$) than conventional *cisplatin* ($\text{IC}_{50} = 20.3 \mu\text{M}$); IC_{50} stands for the half maximal

inhibitory concentration. Contrary, the complexes **2**, **3**, **6**, and **7** showed only comparable in vitro anti-tumor activity with *cisplatin* (Table 3). The in vitro cytotoxicity of the most active complex **8** is more than seven times higher than *cisplatin*. The complexes **1**, **4**, **5**, and **8** were less effective against the A2780R cells than against A2780 ones and their resistance factors (RF; Table 3), defined as the ratio of $IC_{50}(A2780R)/IC_{50}(A2780)$, equalled 1.2–4.6. The complexes **2**, **3**, **6**, and **7** showed comparable or even higher potency against the A2780R cells as compared with A2780 ones, resulting in the RF values of 0.6–1.1 (Table 3). All the studied complexes, except for **1**, showed moderate toxicity against the MRC-5 cells (Table 3). The values of selectivity indexes ($SI = IC_{50}(MRC-5)/IC_{50}(A2780)$) were calculated as being equal to ca. 1.2–9.6 for **1–8**.

2.5. Cell Cycle Analysis

The cell cycle modification was studied by flow cytometry (propidium iodide (PI) staining), using the A2780 cells treated by the IC_{50} concentrations of the representative complexes **1** and **5** (and *cisplatin* for comparative purposes). The obtained results are depicted in Figure 4.

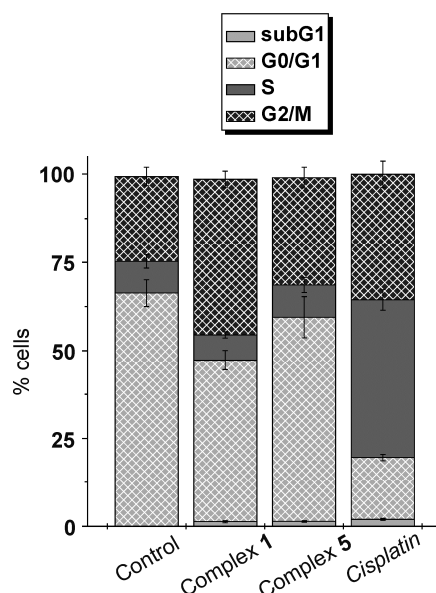


Figure 4. Populations in cell cycle phases studied against the A2780 human ovarian carcinoma cells treated with the complexes **1** and **5**, and *cisplatin* for comparative purposes (control = non-treated cells). Cells were stained with propidium iodide (PI)/RNase. The data are given as the arithmetic mean \pm SD from three independent experiments carried out on cells from three consecutive passages.

Treatment of the A2780 cells by the representative complexes **1** and **5** caused a G_2 cell cycle phase arrest (populations of $44.0\% \pm 2.3\%$ for **1** and $30.4\% \pm 2.9\%$ for **5**), because the % of the populations were higher than in the case of the non-treated A2780 cells (control; $24.0\% \pm 2.6\%$) (Figure 4). The G_2 -arrest was connected with a decrease of the G_0/G_1 cell cycle phase population of the treated A2780 cells ($46.0\% \pm 2.8\%$ for **1** and $58.1\% \pm 5.8\%$ for **5**), as compared with control ($66.3\% \pm 3.8\%$). On the other hand, the S cell cycle phase populations of the cells treated by **1** ($7.2\% \pm 0.9\%$) and **5** ($9.1\% \pm 2.1\%$) were comparable with the control cells ($9.0\% \pm 1.9\%$), but considerably different from *cisplatin* ($44.8\% \pm 2.9\%$).

3. Discussion

Although the complex **1** was previously reported by Chan et al. [28], we decided to use a different synthetic procedure for the syntheses of the studied triphenylphosphane-gold(I) complexes **1–8**. The reported protocol [28] used silver(I) triflate to precipitate the chloride anions released from

[AuCl(PPh₃)] after the addition of Haza deprotonated in situ by triethylamine. In contrast to this protocol, NaOH was used in this work to deprotonate the 7-azaindoles, allowing the isolation of NaCl, which formed as a side product of the performed reactions, as previously reported in the literature (Figure 1) [19,30]. The main reason is that previously used silver(I) triflate could cause unwanted silver contamination for the below-described biological studies.

The N1-coordination mode of the used *naza* ligands was proved for the crystallographically characterized complexes [Au(3I5Braza)(PPh₃)] (7) and [Au(2Me4Claza)(PPh₃)]·½H₂O (8') (Figure 2). Moreover, the results of multinuclear and 2D NMR studies confirmed this coordination mode also for the studied complexes 1–6, because their ¹H-NMR and ¹³C-NMR coordination shift values (defined as $\Delta\delta = \delta_{\text{complex}} - \delta_{\text{ligand}}$; ppm) were consistent with the mentioned 7 and 8. On the other hand, the observation of the negative $\Delta\delta$ values detected for all the aromatic C–H hydrogens of the *naza* ligands points out a different coordination mode from previously-reported platinum(II) or ruthenium(II) complexes containing the electroneutral 7-azaindole-based *N*-donor ligands coordinated through the N7 nitrogen atom [25–27]. The complexes were also characterized by ³¹P-NMR, however, a comparison of the ³¹P-NMR signal positions of 1–8 with the [AuCl(PPh₃)] precursor was prevented by the low stability of [AuCl(PPh₃)] in DMF-*d*₇ (two signals were detected at 33.7 and 25.6 ppm). With respect to this fact, the ³¹P-NMR spectra were recorded also for the CDCl₃ solutions of the representative complex 8 and [AuCl(PPh₃)], both showing one PPh₃ signal at 33.6 ppm and 33.8 ppm, respectively, thus indicating a slight upfield shift as a consequence of the replacement of the chlorido ligand by 2Me4Claza anion.

As it is known for biologically-active substituted-phosphanegold(I) complexes, such as *auranofin*, the mechanism of their action is connected with the ligand displacement [5,36–38]. In particular, the thiolate ligand of *auranofin* is replaced by some of the biomolecules (e.g., albumin, cysteine, or glutathione), while the *P*-donor PET₃ ligand of *auranofin* could be replaced (and subsequently oxidized to urine-excretable O=PET₃) in the excess of some of the mentioned thiols, resulting, for example, in the [Au(SG)₂][−] gold-glutathione adduct [36]. A similar mechanism was also described for [AuCl(PPh₃)], whose interaction with GSH provided the [Au(PPh₃)(SG)] adduct, subsequently releasing its PPh₃ ligand in the presence of GSH or 5,5'-dithiobis-(2-nitrobenzoic acid; dtnb) [15]. For these reasons, we also studied the solution chemistry and interactions with relevant biomolecules for the representative complex 8. The studies of the solution behaviour of 8 in water-containing solution (50% DMF-*d*₇/50% D₂O) showed on its hydrolytic stability, because no new signals were detected in the ¹H and ³¹P-NMR spectra even after 48 h of standing at ambient temperature. Moreover, the position of the signals detected in the ¹H and ³¹P-NMR spectra of 8 differ from those of the starting compounds (H2Me4Claza, PPh₃ or [AuCl(PPh₃)]) or possible product of the decomposition of 8 (O=PPh₃) dissolved in the same mixture of solvents (Figure 3). With respect to these results of ¹H and ³¹P-NMR, we can disclaim that the peak of the {[Au(PPh₃)] + O + 2H}⁺ species detected in the ESI+ mass spectra at 477.0 *m/z* (calcd. 477.1 *m/z*) resulted from the hydrolysis of 8, but its formation is most likely connected with the coordination of water molecule to the [Au(PPh₃)]⁺ species under the electrospray ionization conditions.

The results of the interaction experiment of 8 with GSH (1 molar equivalent) indicated an immediate covalent bonding between both the compounds, probably connected with the formation of the [Au(PPh₃)(SG)] adduct (Figure 3). This is evidenced by the detection of the new Cys-β CH₂ signals [39]; the Cys-α CH signal of the GS–Au adduct was not observed, because it was overlapped by the signal of water. The ³¹P-NMR signal shift is caused by the replacement of 2Me4Claza by SG within a resulting [Au(PPh₃)(SG)] adduct. The signal positions of the released *N*-donor ligand correlated well with those of free H2Me4Claza dissolved in the same mixture of solvents, as depicted in Figure 3. Interestingly, similar experiment performed with 5 mol equiv of GSH did not lead to the release of the coordinated PPh₃ ligand and formation of a [Au(SG)₂][−] adduct, because a) any new ¹H-NMR signals were not detected for glutathione (Figure S7), and b) no ³¹P-NMR signals were detected for the released PPh₃ molecule or its oxidized form (i.e., O=PPh₃; Figure S6). In other words, the ³¹P-NMR spectrum of the complex 8 interacting with an excess of GSH contained only one signal with the same chemical

shift as in the case of the [Au(PPh₃)(SG)] adduct, even after 48 h of standing at ambient temperature. The results of ESI+ mass spectrometry are consistent with those of ¹H and ³¹P-NMR spectroscopy and proved the covalent interaction of the complex **8** with GSH. Similar results were also obtained when the representative complex **8** interacted with another naturally occurring biomolecule, cysteine [40]. This interaction also resulted in the replacement of the *2Me4Claza* ligand by Cys (Figure S8), as proved by ¹H and ³¹P-NMR studies. Again, a considerable downfield shift of the ³¹P-NMR signal of PPh₃ ligand was observed as a consequence of the mentioned changes within the inner coordination sphere. This phenomenon is known from the literature, where the results of the ³¹P-NMR study performed on the [Au(L)(PPh₃)] complexes containing different *N*-donor ligand (L = 4-picoline, 2-amine-4-picoline or *N,N*-dimethylaminopyridine) interacting with *N*-acetyl-L-cysteine (1 mol equiv) in CD₃CN showed similar downfield shift from 30 to ca. 38 ppm [41]. The results of the interaction studies with BSA indicated that the used biomolecule also replaces the *N*-donor ligand *2Me4Claza* in the structure of the representative complex **8** (Figure S8), resulting in the Au-BSA adduct insoluble in the used mixture of solvents (50% DMF-*d*₇/50% D₂O).

The results of the in vitro cytotoxicity testing indicated different potency of **1**, **4**, **5**, and **8** (significantly more potent than *cisplatin*), and **2**, **3**, **6**, and **7** (comparable potency with *cisplatin*) against the A2780 cells (Table 3). Interestingly, although the A2780 cells are naturally sensitive to the biological action of various types of gold(I) complexes including the substituted-phosphane ones (low micromolar or even nanomolar range of the IC₅₀ values), the potency of the previously reported substituted-phosphane-gold(I) complexes is usually comparable or only slightly higher than *cisplatin* [18,21,22,42–45]. In other words, the seven-fold higher in vitro anticancer activity of **8** against the A2780 cells seems to be, to the best of our knowledge, exceptional in the field of gold(I) complexes. Regarding *auranofin*, it showed ca. three-fold higher potency in vitro against the A2780 cells than *cisplatin* [42]. The complexes **1–8** were also tested against the A2780R cancer cell line with acquired resistance to *cisplatin*. The obtained results, calculated as the resistance factors (RF; Table 3), are suggestive for the ability of **2**, **3**, **6**, and **7** to overcome the acquired resistance of the used human ovarian carcinoma cells to the therapeutic action of *cisplatin*, which is comparable with *auranofin* (RF = ca. 0.9) [42] or some other gold(I) complexes reported as effectively circumventing the acquired resistance of the A2780 cells to *cisplatin* [18,45]. Moderate toxicity of the complexes **4**, **5**, and **8** against the MRC-5 normal human fibroblast cells resulted, together with their high cytotoxicity against the A2780 cells, in the promising values (8.3–9.6) of selectivity indexes (SI; Table 3). Selectivity is generally accepted in the field of anticancer potent gold complexes as one of the main advantage of these substances over the conventional platinum-based drugs. For example triphenylphosphane-gold(I) complexes, structurally similar to the complexes **1–8**, which contain 9-deazahypoxanthines as *N*-donor ligand, were reported as compounds showing selective potency towards the cancer cells (especially human MCF-7 breast carcinoma and HOS osteosarcoma cells with SIs up to 30) over the normal cells (human hepatocytes were used) [22]. However, their SI values at the A2780 cells (ca. 4.6–5.2) are lower than for the herein studied complexes **4**, **5**, and **8**. Regarding *auranofin*, its selectivity was very recently reported as comparable with chlorido-triphenylphosphane-gold(I) complex and, more importantly, with *cisplatin*, as resulted from the studies using the B16-F10 metastatic skin melanoma, CT26-WT colon cancer, and 4T1 mammary adenocarcinoma cancer cells and their comparison with non-cancerous BHK21 kidney cells [46].

Both the studied complexes **1** and **5** showed similar trends, but with a different extent of the A2780 cancer cell cycle perturbation (Figure 4). In particular, treatment by the complexes **1** and **5** led to a G₂-arrest, because their populations were higher than those of the non-treated (control) cells. Consequently, the G₀/G₁ population decreased for **1** and **5** as compared with the control cells, while the number of cells in the S cell cycle phase was comparable for **1** and **5**, and the non-treated control cells. Different modification of the A2780 cell cycle, induced by the studied gold(I) complexes (i.e., G₂-arrest) and *cisplatin* (i.e., S-arrest), is indicative for different mechanism of anticancer action of **1** and **5**, as compared with conventional *cisplatin* [47]. The mentioned G₂-arrest observed at the A2780

cells treated by the complexes **1** and **5** is different from the cell cycle modification provoked by different gold(I) complexes including *auranofin*. In particular, *auranofin* induced apoptosis connected with the sub-G₁ cell cycle phase population increase (>13% as compared with untreated cells) in the A549 human lung carcinoma cells [48]. Similar increase of the sub-G₁ population was reported for different triethylphosphane-gold(I) complexes containing CN⁻, SCN⁻ or xanthogenate anion counter-ligand using the 2008 human ovarian carcinoma cells [49]. It is of interest, that *auranofin*, an apoptosis-inducer at the A549 cells (see above), caused the G₀/G₁ cell cycle arrest when it was used for the treatment of the U266 human myeloma cells [50]. The [Au(L)(PPh₃)] complexes (L = 4-picoline, 2-amine-4-picoline or *N,N*-dimethylaminopyridine), structurally similar to the herein studied complexes **1–8**, at the HCT116 human colon carcinoma cells, as well as gold(I) complex of the bis-chelated gold(I)-diphosphane type at the A549 cancer cells, induced the similar increase of the G₀/G₁ cell cycle population [19,44].

Taken together, the treatment of the A2780 cells by the complexes **1** and **5** led the cell cycle to different perturbations, compared to those recently reported for other gold(I) complexes (including *auranofin*) as well as for *cisplatin*. Thus, this observation has to be taken into account as suggestive for a different mechanism of action as compared with the above-named substances.

4. Materials and Methods

4.1. Materials

H[AuCl₄].3H₂O, triphenylphosphane (PPh₃), 7-azaindole (Haza), 3-chloro-7-azaindole (H3Claza), 3-bromo-7-azaindole (H3Braza), 3-iodo-7-azaindole (H3Iaza), 5-bromo-7-azaindole (H5Braza), 3-chloro-5-bromo-7-azaindole (H3Cl5Braza), 3-iodo-5-bromo-7-azaindole (H3I5Braza), 2-methyl-4-chloro-7-azaindole (H2Me4Claza), NaOH, *cisplatin*, reduced glutathione (GSH), cysteine, BSA, Roswell Park Memorial Institute medium, fetal calf serum, glutamine, penicillin and streptomycin, and solvents (acetone, methanol, diethyl ether, chloroform, DMF, DMSO) and solvents for NMR experiments (DMF-*d*₇, D₂O) were supplied by Sigma-Aldrich Co. (Prague, Czech Republic) and Fisher-Scientific Co. (Pardubice, Czech Republic).

The starting chlorido-triphenylphosphane-gold(I) complex, [AuCl(PPh₃)], was prepared as described previously [51], and its composition was checked by elemental analysis and FTIR spectroscopy.

4.2. Synthesis

One mol of NaOH (0.6 mL) was poured into the mixture of [AuCl(PPh₃)] (0.5 mmol) and the appropriate 7-azaindole-based ligand (0.6 mmol) in acetone (10 mL). After 48 h of stirring at 50 °C, the obtained mixtures, containing the white solid, were filtered. The volume of the clear colourless filtrates was reduced until the off-white precipitate formed (**1–4**, **6** and **8**). In the case of the complexes **5** and **7**, the brown gel was obtained when the solvent was removed, which crystalized to the off-white precipitate under diethyl ether. The products (Figure 1) were collected by filtration, washed with diethyl ether (3 × 5 mL), and dried under vacuum.

[Au(aza)(PPh₃)] (**1**): *Anal.* Calcd. for C₂₅H₂₀N₂PAu: C, 51.7; H, 3.6; N, 4.8; Found: C, 51.5; H, 3.6; N, 4.4%. ¹H-NMR (DMF-*d*₇, 400 MHz, 300 K): 8.14 (1H, *m*, C6-H), 7.90 (1H, *m*, C4-H), 7.73 (15H, *m*, PPh₃), 7.52 (1H, *d*, *J* = 3.1 Hz, C2-H), 6.89 (1H, *m*, C5-H), 6.38 (1H, *d*, *J* = 3.1 Hz, C3-H) ppm. ¹³C-NMR (DMF-*d*₇, 100 MHz, 300 K): 160.1 (C7a), 141.6 (C6), 137.7 (C2), 135.2, 135.1, 130.7, 130.6, 129.7 (PPh₃), 127.7 (C4), 122.2 (C3a), 114.8 (C5), 99.8 (C3) ppm. ³¹P-NMR (DMF-*d*₇, 243 MHz, 300 K): 32.7 (P1) ppm.

[Au(3Claza)(PPh₃)] (**2**): *Anal.* Calcd. for C₂₅H₁₉N₂CIPAu: C, 49.2; H, 3.1; N, 4.6; Found: C, 48.9; H, 3.1; N, 4.5%. ¹H-NMR (DMF-*d*₇, 400 MHz, 300 K): 8.24 (1H, *dd*, *J* = 4.6, 1.5 Hz, C6-H), 7.89 (1H, *dd*, *J* = 7.9, 1.3 Hz, C4-H), 7.75 (15H, *m*, PPh₃), 7.63 (1H, *s*, C2-H), 7.03 (1H, *m*, C5-H) ppm. ¹³C-NMR (DMF-*d*₇, 100 MHz, 300 K): 155.6 (C7a), 143.0 (C6), 135.4, 135.2 (PPh₃), 133.3 (C2), 130.8, 130.6, 130.3, 129.7 (PPh₃), 125.4 (C4), 119.5 (C3a), 115.6 (C5), 101.2 (C3) ppm. ³¹P-NMR (DMF-*d*₇, 243 MHz, 300 K): 32.9 (P1) ppm.

[Au(3Braza)(PPh₃)] (3): *Anal.* Calcd. for C₂₅H₁₉N₂BrPAu: C, 45.5; H, 3.0; N, 4.2; Found: C, 45.0; H, 2.9; N, 4.0%. ¹H-NMR (DMF-*d*₇, 400 MHz, 300 K): 8.23 (1H, *m*, C6-H), 7.83 (1H, *m*, C4-H), 7.74 (15H, *m*, PPh₃), 7.65 (1H, *s*, C2-H), 7.04 (1H, *m*, C5-H) ppm. ¹³C-NMR (DMF-*d*₇, 100 MHz, 300 K): 156.2 (C7a), 143.2 (C6), 136.9 (C7), 135.4, 135.3 (PPh₃), 133.4 (C2), 130.8, 130.7, 130.4, 129.9 (PPh₃), 126.2 (C4), 121.1 (C3a), 115.7 (C5), 86.3 (C3) ppm. ³¹P-NMR (DMF-*d*₇, 243 MHz, 300 K): 32.8 (P1) ppm.

[Au(3Iaza)(PPh₃)] (4): *Anal.* Calcd. for C₂₅H₁₉N₂IPAu: C, 42.8; H, 2.7; N, 4.0; Found: C, 42.7; H, 2.4; N, 4.1%. ¹H-NMR (DMF-*d*₇, 400 MHz, 300 K): 8.20 (1H, *d*, *J* = 4.4 Hz, C6-H), 7.72 (17H, *m*, C4-H, C2-H, PPh₃), 7.03 (1H, *dd*, *J* = 7.5, 4.9 Hz, C5-H) ppm. ¹³C-NMR (DMF-*d*₇, 100 MHz, 300 K): 156.8 (C7a), 143.0 (C6), 142.0 (C2), 135.1, 130.7, 130.6, 130.1, 129.7 (PPh₃), 127.7 (C4), 124.2 (C3a), 116.0 (C5), 54.6 (C3) ppm. ³¹P-NMR (DMF-*d*₇, 243 MHz, 300 K): 32.8 (P1) ppm.

[Au(5Braza)(PPh₃)] (5): *Anal.* Calcd. for C₂₅H₁₉N₂BrPAu: C, 45.8; H, 2.9; N, 4.3; Found: C, 45.6; H, 2.8; N, 4.0%. ¹H-NMR (DMF-*d*₇, 400 MHz, 300 K): 8.10 (1H, *s*, C6-H), 8.10 (1H, *s*, C4-H), 7.71 (1H, *s*, C2-H), 7.70 (15H, *m*, PPh₃), 6.65 (1H, *d*, *J* = 2.8 Hz, C3-H) ppm. ¹³C-NMR (DMF-*d*₇, 100 MHz, 300 K): 156.0 (C7a), 141.6 (C6), 139.9 (C2), 135.4, 135.2 (PPh₃), 133.7 (C4), 130.8, 130.7, 129.7 (PPh₃), 124.3 (C3a), 110.1 (C5), 99.9 (C3) ppm. ¹⁵N-NMR (DMF-*d*₇, 40 MHz, 300 K): 276.7 (N7), 188.9 (N1) ppm. ³¹P-NMR (DMF-*d*₇, 243 MHz, 300 K): 33.2 (P1) ppm.

[Au(3Cl5Braza)(PPh₃)] (6): *Anal.* Calcd. for C₂₅H₁₈N₂BrClPAu: C, 43.5; H, 2.6; N, 4.1; Found: C, 43.2; H, 2.6; N, 3.9%. ¹H-NMR (DMF-*d*₇, 400 MHz, 300 K): 8.26 (1H, *s*, C6-H), 8.02 (1H, *s*, C4-H), 7.72 (15H, *m*, PPh₃), 7.72 (1H, *s*, C2-H) ppm. ¹³C-NMR (DMF-*d*₇, 100 MHz, 300 K): 154.0 (C7a), 143.2 (C6), 135.4, 135.3 (PPh₃), 133.4 (C2), 130.8, 130.6, 130.2, 129.8 (PPh₃), 127.4 (C4), 121.1 (C3a), 110.8 (C5), 101.0 (C3) ppm. ³¹P-NMR (DMF-*d*₇, 243 MHz, 300 K): 33.1 (P1) ppm.

[Au(3I5Braza)(PPh₃)] (7): *Anal.* Calcd. for C₂₅H₁₈N₂BrIPAu: C, 38.3; H, 2.4; N, 3.6; Found: C, 38.1; H, 2.1; N, 3.8%. ¹H-NMR (DMF-*d*₇, 400 MHz, 300 K): 8.23 (1H, *d*, *J* = 2.2 Hz, C6-H), 7.73 (17H, *m*, C4-H, C2-H, PPh₃) ppm. ¹³C-NMR (DMF-*d*₇, 100 MHz, 300 K): 152.2 (C7a), 144.2 (C6), 143.10 (C2), 135.3, 135.1 (PPh₃), 132.8 (C4), 130.8, 130.7, 130.2, 129.8 (PPh₃), 126.0 (C3a), 111.1 (C5), 55.6 (C3) ppm. ³¹P-NMR (DMF-*d*₇, 243 MHz, 300 K): 32.8 (P1) ppm.

[Au(2Me4Claza)(PPh₃)] (8): *Anal.* Calcd. for C₂₅H₁₉N₂BrPAu: C, 50.0; H, 3.4; N, 4.5; Found: C, 49.7; H, 3.3; N, 4.4%. ¹H-NMR (DMF-*d*₇, 400 MHz, 300 K): 7.97 (1H, *m*, C6-H), 7.74 (15H, *m*, PPh₃), 6.93 (1H, *m*, C5-H), 6.19 (1H, *s*, C3-H), 2.59 (3H, *s*, CH₃) ppm. ¹³C-NMR (DMF-*d*₇, 100 MHz, 300 K): 158.9 (C7a), 148.0 (C2), 141.0 (C6), 135.4, 135.3 (PPh₃), 133.4 (C4), 130.8, 130.7, 130.4, 130.0 (PPh₃), 122.3 (C3a), 114.3 (C5), 96.7 (C3), 18.1 (CH₃) ppm. ¹⁵N-NMR (DMF-*d*₇, 40 MHz, 300 K): 269.2 (N7), 203.3 (N1) ppm. ³¹P-NMR (DMF-*d*₇, 243 MHz, 300 K): 33.1 (P1) ppm.

4.3. General Methods

Elemental analysis was carried out using a Flash 2000 CHNS Elemental Analyzer (Thermo Scientific, Waltham, MA, USA). ¹H and ¹³C-NMR spectroscopy, and ¹H-¹H gsCOSY, ¹H-¹³C gsHMQC and ¹H-¹³C gsHMBC two-dimensional correlation experiments of the DMF-*d*₇ or CDCl₃ solutions of 1–8 were performed at 300 K on a Varian 400 device (at 400.0 MHz (¹H) or 100.6 MHz (¹³C)); gs = gradient selected, COSY = correlation spectroscopy, HMQC = heteronuclear multiple quantum coherence, HMBC = heteronuclear multiple bond coherence. ¹H and ¹³C-NMR spectra were calibrated against the residual DMF ¹H-NMR (8.03, 2.92 and 2.75 ppm) and ¹³C-NMR (163.2, 34.9 and 29.8 ppm) signals. The splitting of proton resonances in the reported ¹H spectra is defined as s = singlet, d = doublet, dd = doublet of doublets and m = multiplet. ¹H-¹⁵N gsHMBC experiment was carried out at natural abundance for the complex 5 and calibrated against the residual signals of DMF adjusted to 8.03 ppm (¹H) and 104.7 (¹⁵N) ppm. ³¹P-NMR spectra were recorded for the complex 8 (and [AuCl(PPh₃)]) and calibrated against 85% H₃PO₄ used as an internal reference standard. Electrospray ionization mass spectrometry (ESI-MS) was performed by LCQ Fleet ion trap spectrometer (Thermo Scientific; QualBrowser software, version 2.0.7) in both the positive (ESI+) and negative

(ESI[−]) ionization modes on the methanol solutions. FTIR spectra were recorded by a Nexus 670 FT-IR spectrometer (Thermo Nicolet, Waltham, MA, USA) at 150–600 cm^{−1} (far-IR) and 400–4000 cm^{−1} (mid-IR), using the ATR technique. Raman spectroscopy was performed on a NXR FT-Raman Module (Thermo Nicolet, Waltham, MA, USA) between 250 and 3700 cm^{−1}.

4.4. Single Crystal X-ray Analysis

The crystals of the complexes [Au(3I5Braza)(PPh₃)] (**7**) and [Au(2Me4Claza)(PPh₃)]·½H₂O (**8'**) suitable for a single crystal X-ray analysis were prepared by slow evaporation of the solutions of the named complexes in the mixture of dichloromethane and *n*-hexane (1:1, *v/v*). X-ray data of both crystals were collected on a Bruker (Billerica, MA, USA) D8 QUEST diffractometer equipped with a PHOTON 100 CMOS detector (Bruker) using Mo-K_α radiation. The APEX3 software package was used for data collection and reduction [52]. The structures were solved using a direct method and refined using the Bruker SHELXTL Software Package [53]. The graphics were drawn and additional structural calculations were performed using DIAMOND [54] and Mercury [55] software.

4.5. Studies of Aqueous Chemistry and Interaction with Biomolecules

Complex **8** and [AuCl(PPh₃)] (for comparative purposes) were dissolved in 600 μL of the 50% DMF-*d*₇/50% D₂O mixture to give the solutions of ca. 1 mM concentration; a presence of DMF ensured the solubility of the complex **8**, with respect to its low solubility in water. Similar solutions were prepared with **1** or **5** mol equivs of GSH, Cys, or BSA. ¹H and ³¹P-NMR spectra were recorded at different time points over 48 h at 300 K. The obtained ¹H-NMR spectra were calibrated against the residual signal of water found at 4.75 ppm, while the ³¹P-NMR spectra were referenced as described above.

Similar experiments were carried out also in non-deuterated solvents and evaluated by ESI+ mass spectrometry.

4.6. In Vitro Cytotoxicity Testing

Human A2780 ovarian carcinoma, A2780R *cisplatin*-resistant ovarian carcinoma and MRC-5 normal fibroblast cell lines were supplied by the European Collection of Cell Cultures (ECACC). The cell lines were cultured, according to the supplier's instructions, in RPMI-1640 medium supplemented with 10% of fetal calf serum, 1% of 2 mM glutamine, and 1% penicillin/streptomycin. All cell lines were grown as adherent monolayers at 37 °C and 5% CO₂ in a humidified atmosphere.

An appropriate amount of the complexes **1–8** (or *cisplatin* involved in the study as standard) was dissolved in DMF to give the 50 mM stock solutions. The cells were seeded to 96-well culture plates, pre-incubated in drug-free medium at 37 °C for 24 h and treated with the 0.01–10.0 μM solutions (for the complex **1** being less soluble in the used medium) or 0.01–50.0 μM solutions (for sufficiently soluble complexes **2–8** and *cisplatin*) prepared from the stock solutions by dilution with medium, for 24 h at 37 °C. In parallel, the cells were also treated with vehicle (0.1% DMF in medium; negative control) and Triton X-100 (1%; positive control) to assess the minimal and maximal cell damage, respectively. The MTT assay was used to determine the cell viability. A concentration of the formed dye was evaluated spectrophotometrically at 540 nm (TECAN, Schoeller Instruments LLC, Brno, Czech Republic). The data were expressed as the percentage of viability, where 100% and 0% represent the treatments with negative and positive controls, respectively. The data were acquired from three independent experiments (conducted in triplicate) using cells from different passages. The resulting IC₅₀ values (μM) were calculated from viability curves and the results are presented as the arithmetic mean ± SD.

4.7. Cell Cycle Analysis

A2780 cells (1.0 × 10⁶ per well) were pre-incubated in a six-well plate for 24 h, as described above. The selected complexes **1** and **5** were added at the concentrations equal to their IC₅₀

(*cisplatin* was involved in the study for comparative purposes). After 24 h, floating cells were collected and attached cells were harvested using trypsin/EDTA in PBS. Total cells were washed twice with PBS and fixed in 70% ethanol. Cells were resuspended in PBS and DNA staining was achieved by a solution of propidium iodide (PI) supplemented with RNase A (30 min, 25 °C, in the dark). After that, the cells were washed (PBS), resuspended (PBS), and DNA content was measured using flow cytometry (CytoFlex, Beckman Coulter, Brea, CA, USA) detecting emission of DNA-bound PI (maximum at 617 nm) after excitation at 535 nm. The data were analysed using CytExpert™ software (Beckman Coulter).

4.8. Statistical Analysis

An analysis of variance (ANOVA) test was used for statistical analysis with the values of $p < 0.05$ (*), 0.01 (**), and 0.005 (***) considered to be statistically significant. QC Expert 3.2 Statistical software (TriloByte Ltd., Crewe, UK) was used to perform the analysis.

5. Conclusions

In the present work, eight triphenylphosphane-gold(I) complexes containing the deprotonated 7-azaindole or its variously substituted derivatives (*naza*) were investigated. Complexes [Au(3*I5*Braza)(PPh₃)] (7) and [Au(2*Me4*Claza)(PPh₃)]·½H₂O (8') were crystallographically characterized, showing the used 7-azaindole derivatives as coordinated through their N1 atoms. The complexes 4, 5, and 8 exhibited low-micromolar in vitro anticancer potency against the A2780 cells (IC₅₀ = 2.8–3.5 µM; 24 h exposure time), which is significantly higher than that of *cisplatin*. These complexes were markedly less effective (IC₅₀ = 26.0–29.2 µM) against the MRC-5 cells, which is suggestive for promising selectivity towards cancer cells over the normal ones. The treating of the A2780 cells by the representative complexes 1 and 5 (IC₅₀ concentrations were used) led to different cell cycle modification (G2-arrest) as compared with the cells treated by the conventional platinum-based anticancer drug *cisplatin*. The representative complex 8 was hydrolytically stable in the water-containing solution (50% DMF-*d*₇/50% D₂O mixture), while it released its *N*-donor ligand when mixed with relevant naturally occurring biomolecules, i.e., reduced glutathione, cysteine, or bovine serum albumin, as proved by the detailed ¹H and ³¹P-NMR, and ESI+ MS studies.

Supplementary Materials: The following are available online at www.mdpi.com/1422-0067/17/12/2084/s1.

Acknowledgments: The authors gratefully thank the National Program of Sustainability I (LO1305) of the Ministry of Education, Youth and Sports of the Czech Republic for the financial support. The authors also thank Ms. Kateřina Kubešová for performing the in vitro cytotoxicity experiments and preparation of the samples for flow cytometry experiments, Radka Kříkavová for recording the NMR, FTIR and Raman spectra and Mrs. Pavla Richterová for performing elemental analyses. The authors also thank Ms. Pavla Vybíralová for her help with the syntheses of the studied complexes.

Author Contributions: Pavel Štarha, Zdeněk Dvořák and Zdeněk Trávníček conceived and designed the experiments; Pavel Štarha, Bohuslav Drahoš and Zdeněk Trávníček performed the experiments; Pavel Štarha, Bohuslav Drahoš, Zdeněk Dvořák and Zdeněk Trávníček analysed the data; Pavel Štarha and Zdeněk Trávníček wrote the paper. All authors read and approved the final manuscript.

Conflicts of Interest: The authors declare no conflict of interests.

References

1. Gielen, M.; Tiekink, E.R.T. *Metallotherapeutic Drugs and Metal Based Diagnostic Agents*; Wiley: New York, NY, USA, 2005.
2. Mjos, K.D.; Orvig, C. Metallodrugs in medicinal inorganic chemistry. *Chem. Rev.* **2014**, *114*, 4540–4563. [[CrossRef](#)] [[PubMed](#)]
3. Barry, N.P.E.; Sadler, P.J. Exploration of the medical periodic table: Towards new targets. *Chem. Commun.* **2013**, *49*, 5106–5131. [[CrossRef](#)] [[PubMed](#)]

4. Kelland, L. The resurgence of platinum-based cancer chemotherapy. *Nat. Rev. Cancer* **2007**, *7*, 573–584. [[CrossRef](#)] [[PubMed](#)]
5. Shaw, C.F., III. Gold-Based therapeutic agents. *Chem. Rev.* **1999**, *99*, 2589–2600. [[CrossRef](#)]
6. Nardon, C.; Pettenuzzo, N.; Fregona, D. Gold complexes for therapeutic purposes: An updated patent review (2010–2015). *Curr. Med. Chem.* **2016**, *23*, 3374–3403. [[CrossRef](#)] [[PubMed](#)]
7. Ott, I. On the medicinal chemistry of gold complexes as anticancer drugs. *Coord. Chem. Rev.* **2009**, *253*, 1670–1681. [[CrossRef](#)]
8. Zou, T.; Tung Lum, C.; Lok, C.N.; Zhang, J.J.; Che, C.M. Chemical biology of anticancer gold(III) and gold(I) complexes. *Chem. Soc. Rev.* **2015**, *44*, 8786–8801. [[CrossRef](#)] [[PubMed](#)]
9. University of Kansas. Phase I and II Study of Auranofin in Chronic Lymphocytic Leukemia (CLL). US National Institutes of Health. Available online: <https://clinicaltrials.gov/ct2/show/NCT01419691> (accessed on 23 September 2016).
10. Roder, C.; Thomson, M.J. Auranofin: Repurposing an old drug for a golden new age. *Drugs R. D.* **2015**, *15*, 13–20. [[CrossRef](#)] [[PubMed](#)]
11. Mayo Clinic Cancer Center. Auranofin in Treating Patients with Recurrent Epithelial Ovarian, Primary Peritoneal, or Fallopian Tube Cancer. US National Institutes of Health. Available online: <https://clinicaltrials.gov/ct2/show/NCT01747798> (accessed on 23 September 2016).
12. Gromer, S.; Arscott, L.D.; Williams, C.H.; Schirmer, R.H.; Becker, K. Human placenta thioredoxin reductase. *J. Biol. Chem.* **1998**, *273*, 20096–20101. [[CrossRef](#)] [[PubMed](#)]
13. Coffey, M.T.; Shaw, C.F., III; Eidsness, M.K.; Watkins, J.W., II; Elder, R.C. Reactions of auranofin and chloro(triethylphosphine)gold with bovine serum albumin. *Inorg. Chem.* **1986**, *25*, 333–339.
14. Coffey, M.T.; Shaw, C.F., III; Hormann, A.L.; Mirabelli, C.K.; Crooke, S.T. Thiol competition for Et₃PAuS-albumin: A nonenzymatic mechanism for Et₃PO formation. *J. Inorg. Biochem.* **1987**, *30*, 177–185. [[CrossRef](#)]
15. Rubbiani, R.; Kitanovic, I.; Alborzinia, H.; Can, S.; Kitanovic, A.; Onambele, L.A.; Stefanopoulou, M.; Geldmacher, Y.; Sheldrick, W.S.; Wolber, G.; et al. Benzimidazol-2-ylidene gold(I) complexes are thioredoxin reductase inhibitors with multiple antitumor properties. *J. Med. Chem.* **2010**, *53*, 8608–8618. [[CrossRef](#)] [[PubMed](#)]
16. Rubbiani, R.; Can, S.; Kitanovic, I.; Alborzinia, H.; Stefanopoulou, M.; Kokoschka, M.; Mönchgesang, S.; Sheldrick, W.S.; Wölfl, S.; Ott, I. Comparative in vitro evaluation of *N*-heterocyclic carbene gold(I) complexes of the benzimidazolylidene type. *J. Med. Chem.* **2011**, *54*, 8646–8657. [[CrossRef](#)] [[PubMed](#)]
17. Wang, Y.; Liu, M.; Cao, R.; Zhang, W.; Yin, M.; Xiao, X.; Liu, Q.; Huang, N. A soluble *bis*-chelated gold(I) diphosphine compound with strong anticancer activity and low toxicity. *J. Med. Chem.* **2013**, *56*, 1455–1466. [[CrossRef](#)] [[PubMed](#)]
18. Messori, L.; Marchetti, L.; Massai, L.; Scaletti, F.; Guerri, A.; Landini, I.; Nobili, S.; Perrone, G.; Mini, E.; Leoni, P.; et al. Chemistry and biology of two novel gold(I) carbene complexes as prospective anticancer agents. *Inorg. Chem.* **2014**, *53*, 2396–2403. [[CrossRef](#)] [[PubMed](#)]
19. Trávníček, Z.; Štarha, P.; Vančo, J.; Šilha, T.; Hošek, J.; Suchý, P.; Pražanová, G. Antiinflammatory active gold(I) complexes involving 6-substituted purine derivatives. *J. Med. Chem.* **2012**, *55*, 4568–4579. [[CrossRef](#)] [[PubMed](#)]
20. Hošek, J.; Vančo, J.; Štarha, P.; Paráková, L.; Trávníček, Z. Effect of 2-chloro-substitution of adenine moiety in mixed-ligand gold(I) triphenylphosphine complexes on anti-inflammatory activity: The discrepancy between the in vivo and in vitro models. *PLoS ONE* **2013**, *8*, e82441. [[CrossRef](#)] [[PubMed](#)]
21. Křikavová, R.; Hošek, J.; Vančo, J.; Hutýra, J.; Dvořák, Z.; Trávníček, Z. Gold(I)-triphenylphosphine complexes with hypoxanthine-derived ligands: In vitro evaluations of anticancer and anti-inflammatory activities. *PLoS ONE* **2014**, *9*, e107373. [[CrossRef](#)] [[PubMed](#)]
22. Vančo, J.; Gálíková, J.; Hošek, J.; Dvořák, Z.; Paráková, L.; Trávníček, Z. Gold(I) complexes of 9-deazahypoxanthine as selective antitumor and antiinflammatory agents. *PLoS ONE* **2014**, *9*, e109901. [[CrossRef](#)] [[PubMed](#)]
23. Domínguez-Martín, A.; del Pilar Brandi-Blanco, M.; Matilla-Hernández, A.; El Bakkali, H.; Nurchi, V.M.; González-Pérez, J.M.; Castiñeiras, A.; Niclós-Gutiérrez, J. Unravelling the versatile metal binding modes of adenine: Looking at the molecular recognition patterns of deaza- and aza-adenines in mixed ligand metal complexes. *Coord. Chem. Rev.* **2013**, *257*, 2814–2838. [[CrossRef](#)]

24. Zhao, S.B.; Wang, S. Luminescence and reactivity of 7-azaindole derivatives and complexes. *Chem. Soc. Rev.* **2010**, *39*, 3142–3156. [[CrossRef](#)] [[PubMed](#)]
25. Štarha, P.; Marek, J.; Trávníček, Z. Cisplatin and oxaliplatin derivatives involving 7-azaindole: Structural characterisations. *Polyhedron* **2012**, *33*, 404–409. [[CrossRef](#)]
26. Štarha, P.; Trávníček, Z.; Popa, A.; Popa, I.; Muchová, T.; Brabec, V. How to modify 7-azaindole to form cytotoxic Pt(II) complexes: Highly in vitro anticancer effective cisplatin derivatives involving halogeno-substituted 7-azaindole. *J. Inorg. Biochem.* **2012**, *115*, 57–63. [[CrossRef](#)] [[PubMed](#)]
27. Štarha, P.; Hanousková, L.; Trávníček, Z. Organometallic half-sandwich, dichloridoruthenium(II) complexes with 7-azaindoles: Synthesis, characterization and elucidation of their anticancer inactivity against A2780 cell line. *PLoS ONE* **2015**, *10*, e0143871. [[CrossRef](#)] [[PubMed](#)]
28. Chan, C.K.; Guo, C.X.; Cheung, K.K.; Li, D.; Che, C.M. A luminescent heterometallic Au^I...Cu^I complex. Spectroscopic properties and crystal structures of [Au(PPh₃)(C₇H₅N₂)] and [(Au(PPh₃)(μ-C₇H₅N₂))₂](C₇H₅N₂ = 7-azaindo1ate). *J. Chem. Soc. Dalton Trans.* **1994**, 3677–3682. [[CrossRef](#)]
29. Peng, S.M.; Lin, Y.N. Structure of Cu^{II} and Co^{II} clusters of 7-azaindolate: [Cu₂(C₇H₅N₂)₄(dmf)₂] (I), [Cu₄(OCH₃)₄(C₇H₅N₂)₄(dmf)₂] (II) and [Co₄O(C₇H₅N₂)₆]·CHCl₃ (III). *Acta Crystallogr.* **1986**, *C42*, 1725–1731. [[CrossRef](#)]
30. Nomiya, K.; Noguchi, R.; Ohsawa, K.; Tsuda, K.; Oda, M. Synthesis, crystal structure and antimicrobial activities of two isomeric gold(I) complexes with nitrogen-containing heterocycle and triphenylphosphine ligands, [Au(L)(PPh₃)] (HL = pyrazole and imidazole). *J. Inorg. Biochem.* **2000**, *78*, 363–370. [[CrossRef](#)]
31. Nakamoto, K. *Infrared Spectra of Inorganic and Coordination Compounds, Part B, Applications in Coordination, Organometallic, and Bioinorganic Chemistry*; Wiley: New York, NY, USA, 1997.
32. Faggianhi, R.; Howard-Locck, H.E.; Lock, C.J.L.; Turner, M.A. The reaction of chloro(triphenylphosphine)gold(I) with 1-methylthymine. *Can. J. Chem.* **1987**, *65*, 1568–1575. [[CrossRef](#)]
33. Allen, F.H. The Cambridge Structural Database: A quarter of a million crystal structures and rising. *Acta Crystallogr. B Struct. Sci.* **2002**, *58*, 380–388. [[CrossRef](#)]
34. Brammer, L.; Bruton, E.A.; Sherwood, P. Understanding the behavior of halogens as hydrogen bond acceptors. *Cryst. Growth Des.* **2001**, *1*, 277–290. [[CrossRef](#)]
35. Lu, Y.; Shi, T.; Wang, Y.; Yang, H.; Yan, X.; Luo, X.; Jiang, H.; Zhu, W. Halogen bonding—A novel interaction for rational drug design? *J. Med. Chem.* **2009**, *52*, 2854–2862. [[CrossRef](#)] [[PubMed](#)]
36. Roberts, J.R.; Shaw, C.F., III. Inhibition of erythrocyte selenium-glutathione peroxidase by auranofin analogues and metabolites. *Biochem. Pharmacol.* **1998**, *55*, 1291–1299. [[CrossRef](#)]
37. Graham, G.G.; Champion, G.D.; Ziegler, J.B. The cellular metabolism and effects of gold complexes. *Metal-Based Drugs* **1994**, *1*, 395–404. [[CrossRef](#)] [[PubMed](#)]
38. Bhabak, K.P.; Bhuyan, B.J.; Mughesh, G. Bioinorganic and medicinal chemistry: Aspects of gold(I)-protein complexes. *Dalton Trans.* **2011**, *40*, 2099–2111. [[CrossRef](#)] [[PubMed](#)]
39. Smith, W.E.; Reglinski, J.; Hoey, S.; Brown, D.H.; Sturrock, R.D. Action of sodium gold(I) thiomalate on erythrocyte membrane. *Inorg. Chem.* **1990**, *29*, 5190–5196. [[CrossRef](#)]
40. Salemi, G.; Gueli, M.C.; D'Amelio, M.; Saia, V.; Mangiapane, P.; Aridon, P.; Ragonese, P.; Lupu, I. Blood levels of homocysteine, cysteine, glutathione, folic acid, and vitamin B12 in the acute phase of atherothrombotic stroke. *Neurol. Sci.* **2009**, *30*, 361–364. [[CrossRef](#)] [[PubMed](#)]
41. Abbehausen, C.; Peterson, E.J.; de Paiva, R.E.F.; Corbi, P.P.; Formiga, A.L.B.; Qu, Y.; Farrell, N.P. Gold(I)-phosphine-*N*-heterocycles: Biological activity and specific (ligand) interactions on the C-Terminal HIVNCp7 zinc finger. *Inorg. Chem.* **2013**, *52*, 11280–11287. [[CrossRef](#)] [[PubMed](#)]
42. Guidi, F.; Landini, I.; Puglia, M.; Magherini, F.; Gabbiani, C.; Cinellu, M.A.; Nobili, S.; Fiaschi, T.; Bini, L.; Mini, E.; et al. Proteomic analysis of ovarian cancer cell responses to cytotoxic gold compounds. *Metallomics* **2012**, *4*, 307–314. [[CrossRef](#)] [[PubMed](#)]
43. Barreiro, E.; Casas, J.S.; Couce, M.D.; Sánchez, A.; Sánchez-Gonzalez, A.; Sordo, J.; Varela, J.M.; Vázquez López, E.M. Synthesis, structure and cytotoxicity of triphenylphosphinegold(I) sulfanylpropenoates. *J. Inorg. Biochem.* **2008**, *102*, 184–192. [[CrossRef](#)] [[PubMed](#)]
44. Casas, J.S.; Castellano, E.E.; Couce, M.D.; Crespo, O.; Ellena, J.; Laguna, A.; Sánchez, A.; Sordo, J.; Taboada, C. Novel gold(I) 7-azacoumarin complex: Synthesis, structure, optical properties, and cytotoxic effects. *Inorg. Chem.* **2007**, *46*, 6236–6238. [[CrossRef](#)] [[PubMed](#)]

45. Casas, J.S.; Castellano, E.E.; Couce, M.D.; Ellena, J.; Sánchez, A.; Sordo, J.; Taboada, C. A gold(I) complex with a vitamin K3 derivative: Characterization and antitumoral activity. *J. Inorg. Biochem.* **2006**, *100*, 1858–1860. [[CrossRef](#)] [[PubMed](#)]
46. Garcia, A.; Machado, R.C.; Grazul, R.M.; Paz Lopes, M.T.; Corrêa, C.C.; Dos Santos, H.F.; de Almeida, M.V.; Silva, H. Novel antitumor adamantane–azole gold(I) complexes as potential inhibitors of thioredoxin reductase. *J. Biol. Inorg. Chem.* **2016**, *21*, 275–292. [[CrossRef](#)] [[PubMed](#)]
47. Muchová, T.; Prachařová, J.; Štarha, P.; Olivová, R.; Vrána, O.; Benešová, B.; Kašpárková, J.; Trávníček, Z.; Brabec, V. Insight into the toxic effects of *cis*-dichloridoplatinum(II) complexes containing 7-azaindole halogeno derivatives in tumor cells. *J. Biol. Inorg. Chem.* **2013**, *18*, 579–589. [[CrossRef](#)] [[PubMed](#)]
48. Fan, C.; Zheng, W.; Fu, X.; Li, X.; Wong, Y.S.; Chen, T. Enhancement of auranofin-induced lung cancer cell apoptosis by selenocystine, a natural inhibitor of TrxR1 in vitro and in vivo. *Cell Death Dis.* **2014**, *5*, e1191. [[CrossRef](#)] [[PubMed](#)]
49. Gandin, V.; Fernandes, A.P.; Rigobello, M.P.; Dani, B.; Sorrentino, F.; Tisato, F.; Björnstedt, M.; Bindoli, A.; Sturaro, A.; Rella, R.; et al. Cancer cell death induced by phosphine gold(I) compounds targeting thioredoxin reductase. *Biochem. Pharmacol.* **2010**, *79*, 90–101. [[CrossRef](#)] [[PubMed](#)]
50. Nakaya, A.; Sagawa, M.; Muto, A.; Uchida, H.; Ikeda, Y.; Kizaki, M. The gold compound auranofin induces apoptosis of human multiple myeloma cells through both down-regulation of STAT3 and inhibition of NF- κ B activity. *Leukemia Res.* **2011**, *35*, 243–249. [[CrossRef](#)] [[PubMed](#)]
51. Mann, F.G.; Wells, A.F.; Purdie, D. The constitution of complex metallic salts: Part IV. The constitution of the phosphine and arsine derivatives of silver and aurous halides. The coordination of the coordinated argentous and aurous complex. *J. Chem. Soc.* **1937**, 1828–1836. [[CrossRef](#)]
52. Bruker. *Apex3*; Bruker AXS Inc.: Madison, WI, USA, 2015.
53. Sheldrick, G.M. Crystal structure refinement with SHELXL. *Acta Crystallogr. C* **2015**, *71*, 3–8. [[CrossRef](#)] [[PubMed](#)]
54. Brandenburg, K. *Diamond Version 4.0.3*; Crystal Impact GbR: Bonn, Germany, 2015.
55. Macrae, C.F.; Bruno, I.J.; Chisholm, J.A.; Edgington, P.R.; McCabe, P.; Pidcock, E.; Rodriguez-Monge, L.; Taylor, R.; van de Streek, J.; Wood, P.A. Mercury CSD 2.0—New features for the visualization and investigation of crystal structures. *J. Appl. Cryst.* **2008**, *41*, 466–470. [[CrossRef](#)]



© 2016 by the authors; licensee MDPI, Basel, Switzerland. This article is an open access article distributed under the terms and conditions of the Creative Commons Attribution (CC-BY) license (<http://creativecommons.org/licenses/by/4.0/>).